Rev. Roum. Sci. Techn.– Électrotechn. et Énerg.
Vol. **71**, *2*, pp. 311–316, Bucarest, 2026

DUAL GEOCHEMICAL GAS MONITORING SENSOR USING ACTIVE TEMPERATURE DISTURBANCE REJECTION METHOD

ZHENG LI[1], WENXI LI[1], JINGNAN CAI[1], JUN LIN[1], CHUNGUANG LI[2], BIAO WANG[3], CHEN CHEN[1*], HENG PIAO[1,4*]

Keywords: Dual gas measurement; Geochemical applications; Active disturbance rejection control; Temperature control; Stability enhancement.

An active temperature disturbance rejection method was developed to address uncertainties in temperature disturbances and to improve stability for field gas measurements. A symmetric convection heat conduction strategy was used to ensure uniform heating of the multipass cell (MPC). Active disturbance rejection control (ADRC) was adopted to address the nonlinear and uncertain temperature disturbance. The temperature fluctuation is less than 0.01℃ in the stable state during field experiments when controlled at 30℃. The maximum temperature fluctuation during gas sample replacement is less than 0.015 °C. For gas measurement results, CO2 and CH4 concentrations were monitored at 2100-3864 ppmv and 99-104 ppmv, respectively. This temperature control method provides a guarantee for field gas monitoring.

1. INTRODUCTION

Geochemical gases carry a large amount of geological information and have gradually developed into an effective tool in the study of geological structures [1,2]. Trace gas concentrations are a sensitive geochemical tracer, especially in the early monitoring and warning of earthquakes [3]. Carbon dioxide (CO_2) and methane (CH_4) are closely related to geological causes and Earth's ecosystems [4,5]. They are two important geochemical gases, and determining their concentration variations is of great significance for geological analysis.

Compared with the current Methods of gas concentration measurement, such as Semiconductor gas sensing technique, non-dispersive infrared (NDIR) spectroscopy, and Fourier transform infrared (FTIR) [6-8], tunable diode laser absorption spectroscopy (TDLAS) has the characteristics of fast response, in-situ measurement, and high sensitivity [9,10]. In addition, compared with photoacoustic spectroscopy (PAS) and cavity ring-down spectroscopy (CRDS) [11,12], TDLAS has stronger stability and is more suitable for in-situ gas detection in the field environment. With the progress and development of modern industrial technology, TDLAS technology has been widely used in in-situ gas monitoring in environmental, marine, energy, biological, and industrial fields [13–17].

The monitoring environment temperature in the field has great uncertainties. The fluctuation of temperature directly affects the intensity of the gas spectral line [18,19]. In addition, the deformation of optics caused by temperature fluctuations is an important factor affecting the long-term stability of gas measurement [20]. Zhu et al. adopted a temperature compensation method based on spectral line intensity for CO_2 concentration measurement. The maximum relative error of 14% CO_2 measurement at 318 K is −2.57% [21]. However, this correction algorithm cannot solve the error caused by the deformation of the MPC and has a poor effect when the temperature difference is extremely large. Using a component to create a stable temperature environment can directly solve the problem and is more universal. Proportional–integral–derivative (PID), as a simple and easily implementable control strategy, is widely used in various scenarios [22–24]. Ren et al. designed a temperature control system by using flexible printed circuit heating and PID control method for carbon isotope measurement. The precision of the MPC temperature controlling system is 0.1°C [25]. Liu et al. used a thermoelectric cooler (TEC) as a heat source and PID control to design a temperature control system. When the temperature is controlled at 40°C, the fluctuation is controlled within ±0.019°C in the lab [26]. In the above research, the stability performance of the temperature control system is slightly poor, and the verification of the ability to resist disturbance is lacking in the field.

In this article, a method for the temperature control of MPC was proposed. A symmetric convection heat conduction strategy and ADRC were adopted to enhance the stability of the system. A gas sensing system using this temperature controlling method was demonstrated, and the performance was verified in the field. The rest of this article is organized as follows. Sensor system configuration and MPC active temperature disturbance rejection control design are introduced in Section 2. Experiment details and verification experiments are presented in Section 3. Discussion is described in Section 4.

2. EXPERIMENT SET UP

2.1. SENSOR SYSTEM CONFIGURATION

The gas sensing system used TDLAS technology to measure CO_2 and CH_4 gases for applications in geochemical monitoring. The schematic of the sensing system is shown in Fig. 1(a), and the physical diagram is shown in Fig. 1(b).

The sensing system mainly included an optical part, an electrical part, and a gas circuit part. In the optical part, time-division multiplexing was used to achieve dual gas detection. The sensing system used a distributed feedback (DFB) laser as the light source for CO_2 and CH_4 detection by using 2008 nm DFB (Norcada, NL2004) and 2329 nm DFB (Norcada, NL2327), respectively. The lasers were coupled by using a fiber coupler and then injected into the MPC. The laser beam was reflected 220 times in the MPC and emitted from the MPC through a designed effective optical path of 41.5m. The exiting lasers were photoelectrically converted by using a photodevice (Thorlabs, PDA10D). In the electrical part, the signal-generating circuit produced two sine waves (4 kHz) and two sawtooth waves (1 Hz), as well as a sine wave (8 kHz). Where the low frequency sine wave and sawtooth wave were added and transmitted to the laser controller

[1] College of Instrumentation & Electrical Engineering, Jilin University, Changchun 130026, China. E-mail: lizheng23@mails.jlu.edu.cn, caijn24@mails.jlu.edu.cn, lin_jun@jlu.edu.cn, cchen@jlu.edu.cn, piaoheng@neepu.edu.cn. lwx23@mails.jlu.edu.cn
[2] College of Biological and Agricultural Engineering, Jilin University, Changchun 130025, China. E-mail: lichunguang@jlu.edu.cn
[3] Changchun Institute of Optics, Fine Mechanics and Physics, Chinese Academy of Sciences, Changchun 130033, China. E-mail: wb5996@163.com
[4] School of Automation Engineering, Northeast Electric Power University, Jilin 132012, China. E-mail: piaoheng@neepu.edu.cn

DOI: 10.59277/RRST-EE.2026.2.24

(Wavelength, LDTC0520). The laser controller realized the current drive of the laser and controlled the laser temperature. The sine wave (8 kHz) was used as a reference signal to extract second harmonics for the lock-in amplifier (Femto, LIA-MV-150). The converted second harmonics signal was collected by using an analog-to-digital converter (ADI, AD7606). The pressure controller controlled the internal pressure of the MPC to 40 Torr and performed gas sampling. The temperature controller implements the temperature control of the optical cavity, which was described in detail below. The MCU (ST, STM32F091) completes the control of each electrical module and data transmission with the PC.

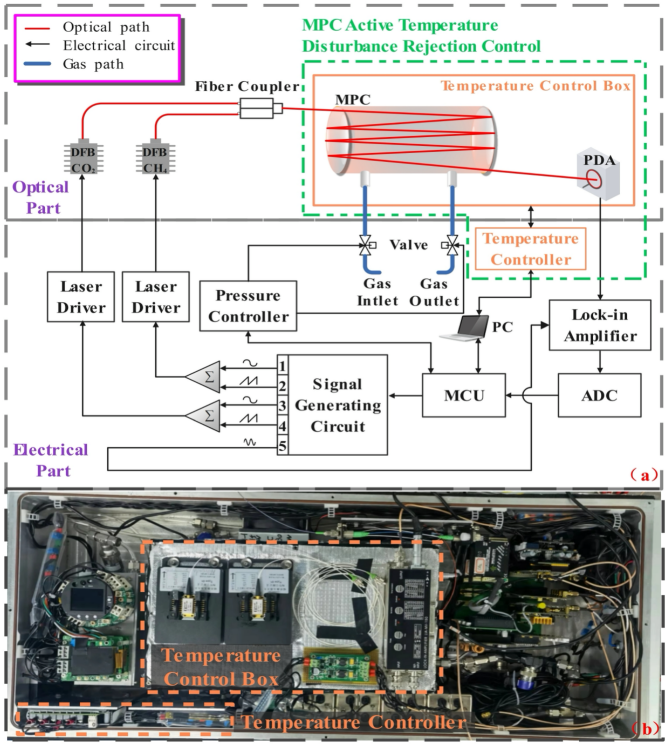

Fig. 1 – Sensor system; a) schematic of the sensing system; b) physical diagram of the sensing system.

2.2. MPC ACTIVE TEMPERATURE DISTURBANCE REJECTION CONTROL DESIGN

2.2.1. MPC TEMPERATURE CONTROL SCHEME DESIGN

Field temperature variation is a major challenge for geochemical gas monitoring. The MPC active temperature disturbance rejection control was designed to keep the temperature of the MPC stable against ambient temperature disturbances, as shown in the green box line in Fig. 1a. A symmetrical convective heat conduction strategy was adopted to complete the temperature control of the MPC in the box. The more detailed temperature control scheme is shown in Fig. 2.

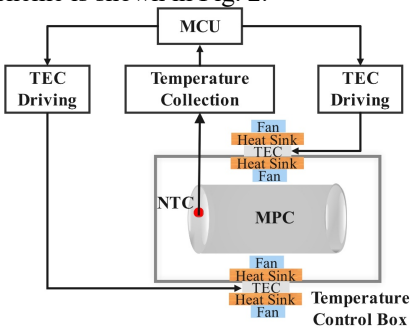

Fig. 2 –MPC Temperature control scheme.

The heat source is a thermoelectric cooler (TEC). In accordance with its working characteristics of absorbing heat at one end and releasing heat at the other end, a combination of a heat sink and a fan was designed at each end of the TEC to complete the heat transfer.

The heat source components were installed on the symmetrical control box to keep the MPC heat transfer even. In the electrical part, a negative temperature coefficient (NTC) thermistor was used as the temperature sensor, and a microcontroller unit (ST, STM32F103ZET6) was used as the controller to collect temperature data and control the TEC.

2.2.2. MPC TEMPERATURE CONTROLLER DESIGN

In accordance with the temperature control system scheme, such a temperature control plant can be reasonably described as a simplified model, as shown in Equation (1) [27].

$$G(s)=\frac{K}{Ts+1}e^{-\tau s}. \quad (1)$$

where K is the gain coefficient, T is the inertia coefficient, and τ is the hysteresis coefficient.

The heat transfer formula as

$$\rho c\frac{\partial t}{\partial \tau}=\frac{\partial}{\partial x}(\lambda\frac{\partial t}{\partial x})+\frac{\partial}{\partial y}(\lambda\frac{\partial t}{\partial y})+\frac{\partial}{\partial z}(\lambda\frac{\partial t}{\partial z})+\dot{\Phi}, \quad (2)$$

where ρ is the density of the volume element, c is the specific heat capacity, the λ is coefficient of thermal conductivity, $\dot{\Phi}$ is the heat of formation per unit volume per unit time. In accordance with the analysis of the thermal

conductivity differential equation shown in Equation (2), the unmodeled part is a complex model and is difficult to establish accurately.

Considering the disturbances to the system, which include ambient temperature changes and gas sampling shocks, establishing the system model is difficult. Thus, the system model is rewritten as

$$\dot{x_1}=\frac{K}{T}u_0-\frac{1}{T}x_1+h(x_1,t)+f(x_1,t), \tag{3}$$

where x_1 is the state variable, u_0 is the input of the plant, $h(x_1,t)$ is the unmodeled part of the system, and $f(x_1,t)$ is the disturbance.

ADRC was used for MPC temperature control by estimating uncertain factors and compensating in real time to address the above uncertainties, as shown in Fig. 3. The ADRC control method mainly consists of an extended state observer (ESO) and a nonlinear feedback controller.

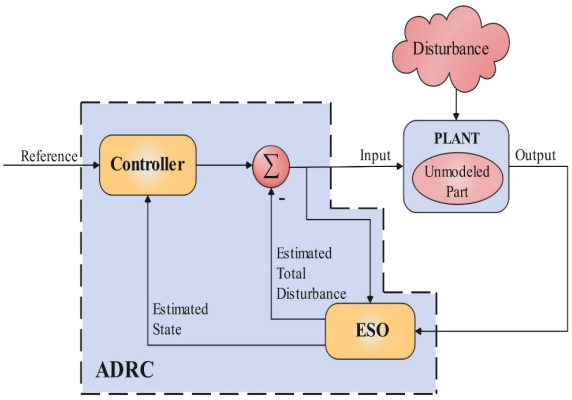

Fig. 3 –Active disturbance rejection control scheme.

The unmodeled part and disturbance are expanded into a new state variable, which is denoted as

$$x_2=h(x_1,t)+f(x_1,t)-\frac{1}{T}x_1(t), \tag{4}$$

Let $\dot{x_2}=\omega(t)$, where $\omega(t)$ is called the total disturbance. eq. (3) is expanded into a new control system:

$$\begin{cases}\dot{x_1}=x_2+\frac{K}{T}u_0\\ \dot{x_2}=\omega(t)\\ y=x_1\end{cases}, \tag{5}$$

where y is the output of the plant. An extended state observer (ESO) was constructed to observe the system state and total disturbance established as

$$\begin{cases}e_0=z_1-y\\ \dot{z_1}=z_2-\beta_{01}fal(e_0,\alpha_0,\delta_0)+bu\\ \dot{z_2}=-\beta_{02}fal(e_0,\alpha_1,\delta_1)\end{cases}, \tag{6}$$

and the nonlinear gain equation is

$$fal(e,\alpha,\delta)=\begin{cases}\frac{e}{\delta^{1-\alpha}} & |e|\le\delta\\ |e|^{\alpha}sgn(e) & |e|>\delta\end{cases}, \tag{7}$$

where u is the output of the controller, z_1 and z_2 are the observed state variables, β_{01}, β_{02} and b are the adjustment gains. The *fal* function is a nonlinear function, where α and δ are adjustment parameters. Compared with linear ADRC, the nonlinear ADRC adopted in this study offers improved transient response and stronger disturbance rejection capability due to the variable-gain characteristics of the *fal* function. However, the parameter tuning and rigorous stability analysis of nonlinear ADRC are more challenging. Extensive research has been conducted on this topic, including bandwidth-parameterization methods and Lyapunov-based stability proofs [28,29]. Since the focus of this work is on practical temperature control for gas sensing rather than control theory, a brief discussion of parameter selection is provided in Subsection 3.1.

Compensation for total disturbance is achieved by selecting the nonlinear error feedback control law as

$$\begin{cases}e=v_r-z_1\\ u=\beta fal(e,\alpha_2,\delta_2)-\frac{z_2}{b}\end{cases}, \tag{8}$$

where v_r is the reference input of the system and β is the adjustment gain.

3. RESULTS AND DISCUSSION

3.1. SIMULATION OF CONTROLLING METHOD

3.1. SIMULATION OF CONTROLLING METHOD

As a traditional general control algorithm, the PID control algorithm has been used as an MPC temperature control algorithm in literature [22,23]. The transfer function of the PID controller is

$$C(s)=k_p+\frac{k_i}{s}+k_d s, \tag{9}$$

where k_p is the proportional gain, k_i is the integral gain and k_d is the derivative gain.

ADRC and PID were simulated in the Simulink software environment to compare the step performance and disturbance rejection ability, as shown in Figure 4. The ADRC parameters were tuned by first determining the compensation gain b, from the identified plant model, then adjusting the ESO bandwidth β_{01} and β_{02}, and finally optimizing the nonlinear function parameters. δ) for transient performance. The parameters for ADRC were as follows: β_{01}=59, β_{02}=0.06, b=0.32, β=4, $\alpha_0=\alpha_1$=0.6, $\delta_0=\delta_1$=0.3, α_2=0.62, and δ_2=0.02. The parameters were k_p=4, k_d=0, and k_i=0.00393 for PID. The plant was given as $G(s)=\frac{3.28}{1025.5s+1}e^{-12.1s}$ through the system identification. The unit step response performance was verified at 0 s, and the step time was set to 0.01 s. As shown in Fig. 4(a), the plant output results showed that ADRC has a faster step performance, reaching steady state at about 270 s. And it took about 460 s for the PID controller. The ordinate is the dimensionless unit of signal amplitude. Step and impulse disturbances were employed to simulate the perturbations induced by ambient temperature variations and changes in the gas source temperature. A step disturbance signal with an amplitude of 0.4 and a duration of 50 s was added at 650 s. A fair comparison was made when the two input control signals had similar amplitude levels, as shown in Fig. 4(b). In the case of adding disturbance, ADRC has better disturbance rejection performance and faster recovery ability,

and the maximum fluctuation is 2.4% smaller than that of PID. When a unit impulse disturbance of amplitude 1 was applied at 1985 s, ADRC reduced the peak fluctuation by 0.63% compared to PID control.

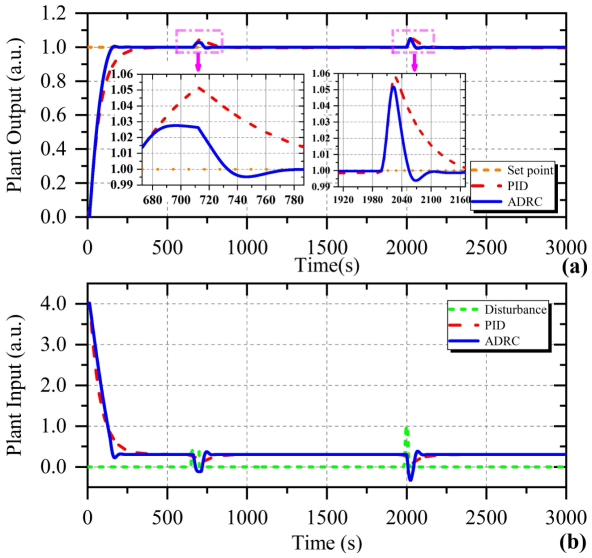

Fig. 4 –Simulation results of the two solutions; a) results of the plant output; b) results of the plant input.

3.2. EXPERIMENT IN THE FIELD

A measurement experiment was conducted at the Fengman Seismic Station in Jilin City, Jilin Province, China, to verify the performance of the gas sensing system in the field.

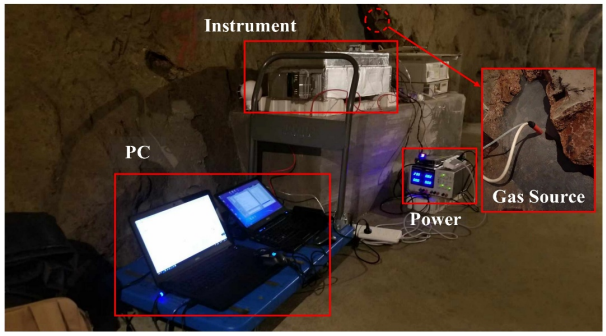

Fig. 5 –Field experiment environment.

The gas overflow was observed through the geochemical observation well in the cave of Fengman Seismic Station. The field experiment site is shown in Fig. 5. The minimum ambient temperature reached 8°C, and the humidity is above 80%. The experiment was continuously monitored for 8 h, and the gas replacement was completed every 60 min. During this process, the CO_2 and CH_4 gas concentrations were measured and recorded.

3.2.1. TEMPERATURE CONTROLLING EXPERIMENT

The target temperature of the temperature control system of the MPC was set to 30°C. The real-time temperature curve is shown in Fig. 6. The temperature control system reached a peak fluctuation of the temperature control system was less than 0.01°C in a stable state. In the subfigure of Fig. 6, the temperature change in the MPC in a gas sample measurement cycle can be observed completely. In the gas sample replacement stage, the temperature of the MPC surface measured by the temperature sensor was slightly higher than the temperature of the gas inside it. The temperature curve rose when the pump pulled out the lower temperature gas.

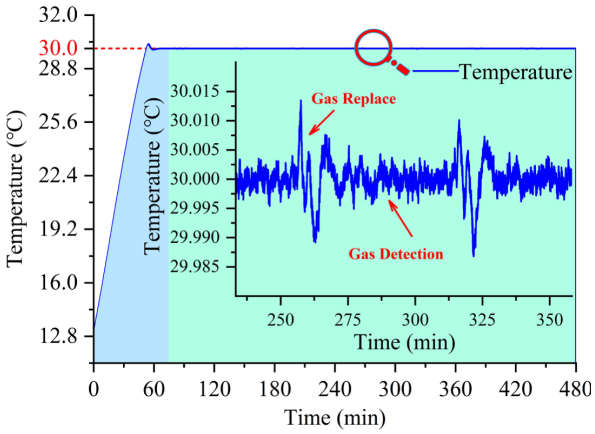

Fig. 6 –MPC temperature control curve in the field experiment.

When the source gas was supplemented into the MPC, the lower temperature gas entered the MPC, causing the temperature to drop. During the gas sample replacement process, the maximum temperature fluctuation was less than 0.015°C. After about 3 min of adjustment, the temperature re-entered a steady state and fluctuated back to less than 0.01°C. To clarify the innovation of the proposed method, the key performance metrics of different control strategies for MPC temperature control are summarized in Table 1. Compared with the PID and fuzzy control methods, which were only validated in laboratory settings, the proposed ADRC strategy achieves superior steady-state performance under real field conditions (steady-state range: 0.01 °C, RMS error and standard deviation: 0.003 °C).

3.2.2. GAS MEASUREMENT EXPERIMENT

When the temperature control system started working, three gas measurements were performed on the same gas sample in the first 60 min. When the temperature control was stable, the gas sample was changed, and measurement was performed every 60 min. The experimental results are shown in Fig. 7.

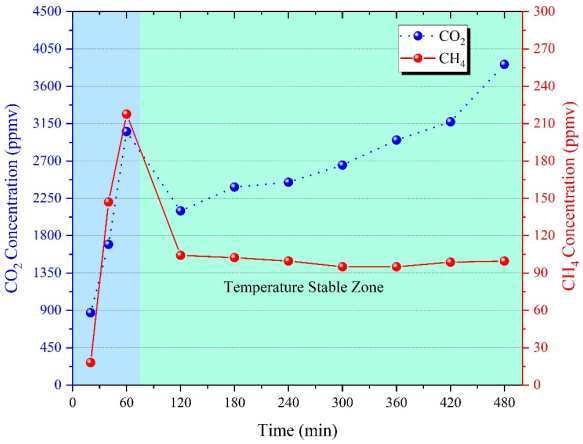

Fig. 7 –CH_4 and CO_2 concentration monitoring in the field experiment.

The measurements of CO_2 and CH_4 concentrations from 0

to 60 min fluctuated greatly due to temperature instability, and the experimental results did not reflect valid geochemical information. During the temperature stable stage, the concentration measurement range of CO_2 was from 2100 ppmv to 3864 ppmv, and CH_4 was from 99 ppmv to 104 ppmv. The concentration of CO_2 showed an upward trend with time during the measurement. This phenomenon might be caused by the gradual strengthening of the respiration of microorganisms in the rock crevices with the measurement cycle time. The concentration of CH_4 was measured with a slow variation and a measurement standard deviation of 3.16 ppmv. The stable CH_4 concentration, which is well above the atmospheric background level, indicates a relatively constant source, such as persistent microbial activity or a deep geological seep [31]. In contrast, the gradual increase in CO_2 likely results from enhanced microbial respiration and the decomposition of organic matter within the soil and rock matrix [32]. Importantly, the absence of correlated drift in the steady CH_4 signal confirms that the observed rise in CO_2 is driven by environmental processes rather than sensor instability, demonstrating the system's ability to resolve genuine geochemical dynamics under field conditions.

Table 1

Performance comparison of different control methods for MPC temperature control.

Ref.	Method	Environment	Steady-State Range (℃)	RMS error (℃)	Std. deviation (℃)	Rise time (s)	Overshoot (℃)
[25]	PID	Lab	0.1	-	-	~10	-
[26]	PID	Lab	0.04	-	0.006	-	-
[30]	Fuzzy	Lab	0.09	-	-	-	-
This work	ADRC	Field	0.01	0.003	0.003	1958.5	0.26

4. **DISCUSSION**

Geochemical gas monitoring is of great significance to earthquake judgment and warning. In this article, a dual gas concentration measurement sensor for CO_2 and CH_4 was constructed via TDLAS. To solve the influence of the uncertainty of the field ambient temperature and air source temperature on gas measurement, a method of active temperature disturbance resistance was used. A symmetric convection heat conduction strategy was designed to ensure uniform heating of the multipass cell (MPC). In addition, the ADRC method was used to estimate temperature disturbance and compensate it in real time. Simulation experiment showed that ADRC had a faster step performance and had an anti-interference ability than PID. In a field experiment, the temperature control system had a high stability performance. The fluctuation was less than 0.01°C when the temperature control entered stability. In comparison with other advanced control strategies for precision temperature control, ADRC provides a balanced alternative among advanced control strategies for precision temperature. Fuzzy logic control often requires extensive expert knowledge [33], model predictive control is computationally intensive for embedded systems [34], and sliding mode control can induce detrimental chattering in thermal components [35]. In contrast, ADRC utilizes a model-agnostic framework where its ESO actively estimates and compensates for combined slow and fast disturbances. This yields robust performance, moderate computational cost, and a smooth control signal, making ADRC well-suited for resource-constrained, field-deployed sensors demanding long-term stability. When replacing the low-temperature gas, the maximum temperature fluctuation was less than 0.015°C. The temperature control method effectively guaranteed the measurement of CO_2 and CH_4 gases and improved the measurement stability of the sensing system in the face of complex environments. For monitoring of underground gas leakage from rock caves, the sensor measured the concentrations of CO_2 and CH_4 from 2100 ppmv to 3864 ppmv and from 99 ppmv to 104 ppmv.

This study has certain application value for the field monitoring of geochemical gases. The active temperature disturbance rejection method proposed in this paper has stable performance in solving the influence of ambient temperature disturbance on the sensor, and provides a new solution for the spectral sensor to expand the in situ gas detection in other harsh environments.

CREDIT AUTHORSHIP CONTRIBUTION STATEMENT

ZHENG LI: Contribution to experiment and writing, original draft preparation.
WENXI LI: Contribution to data visualization and experiment.
JINGNAN CAI: Contribution to data processing.
JUN LIN: Contribution to offering guidance and subject definition.
CHUNGUANG LI: Contribution to offering guidance and subject definition.
BIAO WANG: Contribution to experiment.
CHEN CHEN: Contribution to writing, review, and editing.
HENG PIAO: Contribution to experiment.

Received on 13 April 2025

REFERENCES

1. H. Ye, Q. Liu, Q. Bao, Z. Wang, Y. Xie, T. Michelle, W. Zhao, C. Xian, *Review on in-situ CO2 mineralization sequestration: mechanistic understanding and research frontiers*, International Journal of Coal Science & Technology, **12**, *1*, pp. 15–31, (2025).
2. Y. Wang, D.R. Hilton, Z. Zhou, G. Zheng, *Progress in the application of gas geochemistry to geothermal, tectonic and magmatic studies*, Chemical Geology, **469**, pp. 1–3, (2017).
3. P. Wang, C. Chen, Y. Wang, D. Cheng, H. Piao, X. Pan, *Improvement of measurement accuracy using state equivalence correction for CH4 and CO2 sensor in geochemical application*, Measurement, **192**, pp. 1–9, (2022).
4. Q. Zhuang, J.M. Melillo, M.C. Sarofim, D.W. Kicklighter, A.D. McGuire, B.S. Felzer, A. Sokolov, R.G. Prinn, P.A. Steudler, S. Hu, *CO2 and CH4 exchanges between land ecosystems and the atmosphere in northern high latitudes over the 21st century*, Geophysical Research Letters, **33**, *17*, pp. 1–5, (2006).
5. C. Lu, W.S. Han, S. Lee, B.J. McPherson, P.C. Lichtner, *Effects of density and mutual solubility of a CO2 -brine system on CO2 storage in geological formations; "warm" vs. "cold" formations*, Advances in Water Resources, **32**, *12*, pp. 1685–1702, (2009).

6. D. Zhang, N. Yin, B. Xia, *Facile fabrication of ZnO nanocrystalline-modified graphene hybrid nanocomposite toward methane gas sensing application*, Journal of Materials Science: Materials in Electronics, **26**, *8*, pp. 5937–5945, (2015).
7. L. Fu, S. You, G. Li, Z. Fan, *Enhancing methane sensing with NDIR technology: Current trends and future prospects*, Reviews in Analytical Chemistry, **42**, *1*, pp. 6–15, (2023).
8. I. Elpelt-Wessel, M. Reiser, D. Morrison, M. Kranert, *Emission determination by three remote sensing methods in two release trials*, Atmosphere, **13**, *1*, pp. 1–15, (2022).
9. H. Piao, D. Cheng, C. Chen, Y. Wang, P. Wang, X. Pan, *A high-accuracy CO2 carbon isotope sensing system using subspace identification of Hammerstein model for geochemical application*, IEEE Transactions on Instrumentation and Measurement, **71**, pp. 1–9, (2022).
10. R. Li, F. Li, X. Lin, X. Yu, *Error analysis of integrated absorbance for TDLAS in a nonuniform flow field*, Applied Sciences, **11**, *22*, pp. 1–15, (2021).
11. Z. Lang, S. Qiao, Y. Ma, *Acoustic microresonator-based in-plane quartz-enhanced photoacoustic spectroscopy sensor with a line interaction mode*, Optics Letters, **47**, *6*, pp. 1295–1298, (2022).
12. S. Song, C. Yan, *Trace methane detection based on cavity ring-down spectroscopy*, Spectroscopy and Spectral Analysis, **40**, *7*, pp. 2023–2028, (2020).
13. F. Xin, J. Li, J. Guo, D. Yang, Y. Wang, Q. Tang, Z. Liu, *Measurement of atmospheric CO2 column concentrations based on open-path TDLAS*, Sensors, **21**, *5*, pp. 1–15, (2021).
14. Z. Zhang, M. Li, J. Guo, B. Du, R. Zheng, *A portable tunable diode laser absorption spectroscopy system for dissolved CO2 detection using a high-efficiency headspace equilibrator*, Sensors, **21**, *1723*, pp. 1–15, (2021).
15. C. Fan, Y. Gao, Y. Hu, M. Liao, J. Wu, C. Chen, *Development of methane carbon isotope based on mid-infrared absorption spectrum technology applied in logging platform*, Rev. Roum. Sci. Techn. – Électrotechn. et Énerg., **68**, *4*, pp. 419–423, (2023).
16. L. Shao, J. Mei, J. Chen, T. Tan, G. Wang, K. Liu, X. Gao, *Simultaneous sensitive determination of δ13C, δ18O, and δ17O in human breath CO2 based on ICL direct absorption spectroscopy*, Sensors, **22**, *1527*, pp. 1–11, (2022).
17. X. Guo, F. Zheng, C. Li, X. Yang, N. Li, S. Liu, J. Wei, X. Qiu, Q. He, *A portable sensor for in-situ measurement of ammonia based on near-infrared laser absorption spectroscopy*, Optics and Lasers in Engineering, **115**, pp. 243–248, (2019).
18. L. Ma, X. Fan, S. Zhang, W. Wang, G. Wei, *Research on CH4 gas detection and temperature correction based on TDLAS technology*, Spectroscopy and Spectral Analysis, **41**, *11*, pp. 3632–3638, (2021).
19. Z. Li, S. Yao, W. Lu, X. Zhu, L. Zou, Y. Li, Z. Lu, *Study on temperature correction method of CO2 measurement by TDLAS*, Spectroscopy and Spectral Analysis, **38**, *7*, pp. 2048–2053, (2018).
20. W. Liang, Q. Zhou, X. Dong, T. Lv, *Influence of temperature-induced cavity length variation in wavelength modulation spectroscopy*, Optik, **172**, pp. 220–224, (2018).
21. X. Zhu, S. Yao, W. Ren, Z. Lu, Z. Li, *TDLAS monitoring of carbon dioxide with temperature compensation in power plant exhausts*, Applied Sciences, **9**, *3*, pp. 1–15, (2019).
22. R. Sekar, M. Arunachalam, K. Subramanian, *Fuzzy-proportional integral derivative controller with interactive decision tree*, Rev. Roum. Sci. Techn. – Électrotechn. et Énerg., **69**, *4*, pp. 395–400, (2024).
23. M. Abdelwanis, A. Zaky, *Maximum power point tracking in a perovskite solar pumping system with a six-phase induction motor*, Rev. Roum. Sci. Techn. – Électrotechn. et Énerg., **69**, *1*, pp. 15–20, (2024).
24. G. Murugaiyan, J. Gnanamalar, M. Narayanaperumal, V. Muthuvel, *Red fox-based fractional order fuzzy PID controller for smart LED driver circuit*, Rev. Roum. Sci. Techn. – Électrotechn. et Énerg., **68**, *4*, pp. 395–400, (2023).
25. Q. Ren, Y. Wang, C. Chen, *A prototype of high-precision carbon isotopic ratio sensing system for CO_2 dissolved in water*, IEEE Transactions on Instrumentation and Measurement, **69**, pp. 9813–9821, (2020).
26. X. Liu, P. Sun, X. Yang, T. Pang, H. Xia, B. Wu, Z. Zhang, Z. Shu, Q. Xu, *High precision temperature control design for TDLAS gas detection system*, Acta Photonica Sinica, **49**, *12*, pp. 99–110, (2020).
27. J. Li, S. Liu, P. Zhang, H. Liu, L. Shao, *PCR instrument temperature control system based on multimodal control*, in 2020 Chinese Control and Decision Conference (CCDC), Hefei, China, pp. 149–154, (2020).
28. J. Han, *From PID to active disturbance rejection control*, IEEE Transactions on Industrial Electronics, **56**, *3*, pp. 900–906, (2009).
29. Z. Gao, *Scaling and bandwidth-parameterization based controller tuning*, in 2003 Conference on American Control, **6**, pp. 4989–4996, (2003).
30. G. Li, F. Zhao, H. Yuan, L. Jia, E. Dong, S. Zhang, G. Cui, Y. Zhao, R. Sun, L. Li, *In-situ ammonia escape measurement sensor integrating a multi-factor spectral signal processing model*, Sensors and Actuators B: Chemical, **424**, pp. 1–8, (2025).
31. E. Nisbet et al., *Atmospheric methane: comparison between methane's record in 2006–2022 and during glacial terminations*, Global Biogeochemical Cycles, **37**, *8*, pp. 1–16, (2023).
32. A. Tune, J. Druhan, J. Wang, P. Bennett, D. Rempe, *Carbon dioxide production in bedrock beneath soils substantially contributes to forest carbon cycling*, Journal of Geophysical Research: Biogeosciences, **125**, *12*, pp. 1–14, (2020).
33. A. Bushnag, S. Chaabane, R. Harrabi, L. Alharabi, M. Alshmrani, S. Abuzneid, *Smart agriculture: IoT-based smart irrigation with advanced fuzzy logic control*, Expert Systems with Applications, **299**, pp. 1–16, (2026).
34. J. Kim, F. You, *Energy-efficient greenhouse climate control using Gaussian process-based stochastic model predictive control*, Applied Energy, **391**, pp. 1–20, (2025).
35. S. Zheng, C. Zhou, K. Mao, *Novel adaptive super-twisting sliding mode observer for the control of the PMSM in the centrifugal compressors of hydrogen fuel cells*, Energies, **18**, *17*, pp. 1–21, (2025).